Aerospace Systems (2024) 7:293–304
https://doi.org/10.1007/s42401-023-00269-8

ORIGINAL PAPER

Finite-time error convergent trajectory generation with field-of-view and angle constraints

Ye Chen[1] · Shufan Wu[1] · Xiaoliang Wang[1] · Di Zhang[2] · Jun Jia[2] · Quan Li[2]

Received: 12 May 2023 / Revised: 30 November 2023 / Accepted: 9 December 2023 / Published online: 12 January 2024

Abstract
A homing guidance law combined with terminal angle constraint and seeker's field-of-view limit is proposed in this paper for hitting a stationary target. The proposed guidance scheme is composed of proportional navigation guidance and a continuous feedback term with respect to a newly defined angle error. Considering that many existing methods use switching logic strategy to address the specific constraint which will generate discontinuous acceleration command, the proposed scheme overcomes the limitation by not using switching logic. Furthermore, the finite-time convergence of angle error before interception is guaranteed via a Lyapunov-like approach, a shaping function is also designed to lengthen the range at which the error becomes zero. Numerical simulations demonstrate the characteristics and advantages of the proposed guidance law.

Keywords Trajectory generation · Finite-time convergence · Field-of-view constraint · Angle constraint

1 Introduction

The terminal guidance of missile aims to intercept the target precisely. To maximize the damage effect and lethality of warhead, the missile usually needs to have a specific attack angle when hitting the target. For the homing guidance problem with angle constraint, different methods have been explored and proposed in recent years. Such as proportional navigation guidance (PNG) with a biased term [1, 2], optimal control-based guidance law [3, 4], H_∞-based guidance law [5], and nonlinear differential game-based guidance law [6].

Finite-time convergence property normally exists in sliding mode control (SMC)-based methods, SMC has been widely explored and applied in homing guidance in recent years because of its strong robustness to system uncertainties and external disturbances [7, 8]. A terminal sliding mode (TSM) guidance law with angle constraint was derived in Ref. [9], the guidance performance was improved by introducing nonlinear sliding manifold. But SMC-based methods can sometimes have singularity problems which show their limitations. In Ref. [10], the switching policy was designed when the terminal sliding manifold was close to the singular region. In Ref. [11], a fast nonsingular terminal sliding manifold was derived, which not only avoids the singularity problem but also improves the convergence rate of the guidance scheme.

To meet the desired attack angle requirements, the missile trajectory is usually curved, which can cause the target to exceed the field of view (FOV) of the missile seeker and consequently, some vital variables like line-of-sight (LOS) angle cannot be measured [12, 13]. In the process of terminal guidance, with the decrease of the relative distance, this problem is more likely to happen. Therefore, the homing guidance law needs to consider the FOV constraint while handling the angle constraint. To solve this problem, a biased PNG was proposed in Ref. [14], and the weighted term was improved in three stages to make the missile meet the two constraints. In Ref. [15], a TSM-based trajectory generation algorithm with attack angle was designed. On the basis of which a FOV angle constraint term was introduced, when the angle was greater than the preset threshold, the FOV angle constraint term was activated to lock the FOV angle value. However, in the works of [14, 15], the switching logic strategies were used to restrict the FOV angle, which make the guidance law have the problem of unreasonable command chattering. In Ref. [16], an analytical algorithm was proposed to address

✉ Ye Chen
chaser_y@sjtu.edu.cn

[1] School of Aeronautics and Astronautics, Shanghai Jiao Tong University, Shanghai 200240, China

[2] Shanghai Electromechanical Engineering Institute, Shanghai 201109, China

the FOV constraint by changing the initial LOS angle or relaxing the attack angle constraint. Since the FOV angle range was constrained by other conditions, the application was reduced. Besides, a size-constrained symbolic function guidance law was designed in Ref. [17] to satisfy the two aforementioned constraints. But the works in Refs. [16, 17] are only applicable to stationary targets.

From the other perspective, the FOV constraint problem can be addressed by introducing error feedback term or transforming it into a state-constrained tracking control problem. In Ref. [18], combined with the integral obstacle Lyapunov function, a novel algorithm was designed, but the selected sliding manifold cannot ensure that the state variables of internal system dynamics are convergent in finite time. In Ref. [19], the integral obstacle Lyapunov function was also used to address the FOV constraint, but the attack angle was not considered, and the introduction of integral term in Refs. [18, 19] makes the solving process of the guidance scheme much difficult, which limits its application. A cooperative homing approach considering FOV constraint was proposed in Ref. [20] for salvo attack, FOV constraint was addressed by a velocity-like constrained consensus algorithm and optimal control was utilized to make that the control effort was minimized. Han et al. [21] proposed an analytical FOV constrained guidance law based on polynomial functions. However, tedious parameter settings were needed in Ref. [21] which was not convenient for practical application. Similar to Refs. [21], [22–24] also derived guidance laws with multiple constraints by introducing polynomial functions. In Ref. [25], a non-switching guidance strategy was proposed for missiles with time-varying speeds considering impact angle, field of view, and input saturation constraints. A first-order filter was designed to compensate the effect of disturbances. Zhou et al. [26] proposed a SMC-based law with the two aforementioned constraints, two types of barrier Lyapunov functions were selected to guarantee the finite-time convergence of sliding manifold.

To sum up, the above noted studies either only consider the angle constraint, or just consider the FOV constraint. And the law with both constraints still have some drawbacks like: switching logic used in the guidance framework, which could unavoidably cause command chattering; linearized angle assumptions used in the engagement model; singularity problem of the law. Different from the above investigations, this paper aims to address the homing guidance problem with both FOV and angle constraints without using switching logic to generate a much smoother guidance command. First of all, the characteristics of PNG are presented, the terminal flight path angle (FPA) of PNG is also derived to be the impact angle of the whole guidance scheme. The guidance command has two components, one is the classical PNG, which can guarantee the missile hit the target and achieve zero miss distance; the other is a feedback term containing angle error. The main contributions of this study are summarized as follows

1. A biased-PNG form guidance law is derived to address the homing guidance problem with angle and FOV constraints.
2. The proposed method generates much smoother and continuous guidance commands without using switching logic or other techniques compared with existing works [3, 4, 6, 14, 15, 27, 28].
3. Finite-time convergence of error can be guaranteed w.r.t. range via a Lyapunov-like approach. This property is different from some existing SMC-based laws that may not ensure the convergence of sliding manifold before interception if the guidance parameters are not properly selected.
4. A shaping function is designed and validated to improve the performance of the law.

The structure of this paper is organized as follows: Sect. 2 gives the formulation of the constrained homing guidance problem. The PNG is further derived in detail in Sect. 3. Based on the derivations, a new guidance law is proposed and analyzed in Sect. 4. Simulations are performed in Sect. 5 to test the performance of the law. Conclusion and future works are drawn in Sect. 6.

2 Problem statement

Consider the guidance scenario that a homing missile attacks a stationary target under FOV and angle constraints. Before theoretical derivations, the following assumptions are made throughout the paper:

Assumption 1 The two participators (missile and target) are regarded as mass points.

Assumption 2 The missile has a constant speed.

Assumption 3 The control loop responds quickly and the autopilot lags can be ignored.

Note that the above assumptions are reasonable and used in many guidance scenarios [12, 15–17]. Accordingly, a planar guidance geometry is shown in Fig. 1.

The two participators are denoted as M and T, respectively. $X_I O_I Y_I$ is the inertial coordinate system. r represents the relative distance between M and T or range-to-go. θ, ϕ, and η represent the line-of-sight (LOS) angle, flight path angle (FPA), and leading angle, respectively. It is assumed that all angles have positive signs under counterclockwise direction. Moreover, the missile's velocity and acceleration are denoted as v_m and a_m, with acceleration vector being

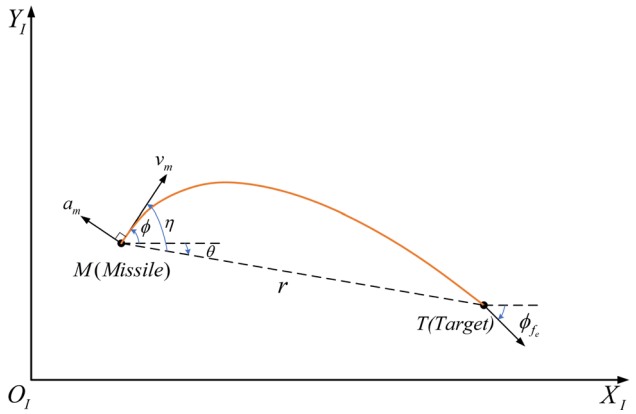

Fig. 1 Engagement geometry

perpendicular to velocity vector. Then the engagement kinematic equations are given as follows

$$\dot{r} = -v_m \cos\eta \tag{1}$$

$$\dot{\theta} = -\frac{v_m \sin\eta}{r} \tag{2}$$

$$\eta = \phi - \theta \tag{3}$$

$$\dot{\phi} = \frac{a_m}{v_m} \tag{4}$$

$$\dot{\eta} = \dot{\phi} - \dot{\theta} = \frac{a_m}{v_m} + \frac{v_m \sin\eta}{r} \tag{5}$$

In terms of impact angle control guidance (IACG), it is hoped that the target is intercepted at an expected impact angle ϕ_{f_e}. To formulate this problem, impact angle error is introduced as follows

$$e_{\phi_f} = \hat{\phi}_f - \phi_{f_e} \tag{6}$$

where $\hat{\phi}_f$ represents the terminal FPA estimate, ϕ_{f_e} is defined prior and is a constant. If e_{ϕ_f} with a reasonable terminal FPA estimate converges to zero before interception, then the IACG is considered to be successfully performed, i.e.,

$$e_{\phi_f} \to 0 \quad \text{as} \quad t \to t_1 < t_f \tag{7}$$

where t_1 is the time instant at which e_{ϕ_f} becomes zero, t_f is the terminal flight time. t_1 should be less than t_f theoretically.

In addition to angle constraint, FOV limit of seeker is also taken into account in this study. If the leading angle varies within the boundaries of FOV limit during the whole engagement, accordingly, the FOV constraint is said to be well satisfied. This problem is formulated by

$$|\eta(t)| \le \eta_{\max} < \frac{\pi}{2} \quad \text{for} \quad t_0 \le t \le t_f \tag{8}$$

where $\eta_{\max}$ is the maximum FOV angle, and is less than 90°. t_0 is the initial flight time.

Remark 1 Notice that the leading angle is chosen as the FOV angle, it is reasonable since the angle of attack (AOA) in the terminal guidance phase is small [27]. The initial leading angle η_0 should not violate the boundaries. Besides, as for intercepting a stationary target, there is a property that $\eta(t_f) = 0$. Besides, the seeker is assumed to have symmetric FOV, i.e., $\eta_{\min} = -\eta_{\max}$.

3 Further analysis and derivation of proportional navigation guidance

In this section, the basic principles of PNG are first presented. With further analysis, the variations of leading angle and acceleration are explored, and the terminal impact angle of PNG is derived.

3.1 Proportional navigation guidance

In this guidance scenario, the analytical guidance command of PNG takes the form

$$a_{m_{PNG}} = N v_m \dot{\theta} \tag{9}$$

where N is the navigation coefficient, and is usually selected as $2 \le N \le 6$. Combining Eq. (2), the guidance command of PNG for intercepting a stationary target can be rewritten as

$$a_{m_{PNG}} = -\frac{N v_m^2 \sin\eta}{r} \tag{10}$$

3.2 Leading angle and acceleration variations of PNG

It is not difficult to find that the leading angle variation can be obtained by substituting Eq. (10) into Eq. (5), which yields

$$\dot{\eta} = -\frac{(N-1) v_m \sin\eta}{r} \tag{11}$$

When $0 < \eta < \pi$, $\dot{\eta} < 0$; when $-\pi < \eta < 0$, $\dot{\eta} > 0$. Thence, conclusion can be drawn that $\frac{d|\eta|}{dt} \le 0$ as $\eta \in (-\pi, \pi)$. Next, consider the relation between r and η, combining Eqs. (1) and (11), the derivative of r w.r.t. η takes the form

$$\frac{dr}{d\eta} = \frac{\dot{r}}{\dot{\eta}} = \frac{r}{N-1}\frac{\cos\eta}{\sin\eta} \tag{12}$$

Integrating Eq. (12) gives the relation between the two variables as follows

$$|\sin\eta| = |\sin\eta_0|\left(\frac{r}{r_0}\right)^{N-1} \tag{13}$$

It can be seen from Eq. (13) that under the condition $N > 1$, when r tends to zero, $\sin\eta$ (i.e., η) will also tend to zero, which validates the property illustrated in Remark 1. Consequently, the magnitude of acceleration command of PNG can be calculated by substituting Eq. (13) into Eq. (10), which takes the form

$$|a_{m_{PNG}}| = N v_m^2 |\sin\eta_0| \frac{r^{N-2}}{r_0^{N-1}} \tag{14}$$

Remark 2 Similar conclusion can be drawn from Eq. (14) that under the condition $N > 2$, $|a_{m_{PNG}}|$ (i.e., $a_{m_{PNG}}$) will tend to zero as $r \to 0$. As for typical homing missile, it is a desirable and good property that the terminal acceleration command equals zero, because it can reduce the energy cost of the whole missile system. And this can be the reason that the classical PNG is still popular in practical engineering. In next section, a biased guidance term will be designed and added to the PNG command, and the property $a_m = 0$ will be our design principle and the strength of the guidance law.

3.3 Derivation of the terminal impact angle of PNG

On account of the angle constraint is considered in the guidance framework, the terminal impact angle of PNG is derived in this subsection for terminal FPA estimate $\hat{\phi}_f$ as introduced in Sect. 1.

Combining Eqs. (3)–(5) and Eq. (9), a new form of leading angle dynamics of PNG can be obtained as follows

$$\dot{\eta} = N\dot{\theta} - \dot{\theta} = (N-1)\dot{\theta} = (N-1)(\dot{\phi} - \dot{\eta}) \tag{15}$$

Integrating Eq. (15) from t_0 to t_f, we have

$$\phi_{f_{PNG}} - \phi = \frac{N}{N-1}(\eta_{f_{PNG}} - \eta) \tag{16}$$

where $\phi_{f_{PNG}}$ and $\eta_{f_{PNG}}$ represent the terminal FPA and leading angle of PNG, respectively. Note that $\eta_{f_{PNG}} = 0$ is guaranteed as illustrated in Remark 1. Thence, the terminal impact angle of PNG which is selected as the terminal FPA can be given by

$$\phi_{f_{PNG}} = \phi - \frac{N}{N-1}\eta, \quad \eta \in [\eta_{\min}, \eta_{\max}] \tag{17}$$

Combining Eq. (3), $\phi_{f_{PNG}}$ can be rewritten in alternative ways as follows

$$\phi_{f_{PNG}} = \phi - \frac{N}{N-1}\eta = \theta - \frac{1}{N-1}\eta, \quad \eta \in [\eta_{\min}, \eta_{\max}] \tag{18}$$

or

$$\phi_{f_{PNG}} = -\frac{1}{N-1}\phi + \frac{N}{N-1}\theta, \quad \eta \in [\eta_{\min}, \eta_{\max}] \tag{19}$$

Remark 3 Note that Eqs. (17)–(19) are valid only if $\eta \in (-\pi, \pi)$, because $\eta = \pm\pi$ will lead to $\dot{\theta} = 0$ and $a_{m_{PNG}} = 0$, and the missile will be guided away from the target which should be avoided. Since the FOV limit is considered in this study, this condition is restricted to $\eta \in [\eta_{\min}, \eta_{\max}]$. In addition, the terminal impact angle of PNG $\phi_{f_{PNG}}$ is regarded as the terminal FPA estimate $\hat{\phi}_f$ as defined in Eq. (6) for further derivation.

4 Field-of-view limited guidance law with angle constraint

In this section, for stationary target, a FOV limited guidance law with angle constraint is proposed. The law takes the form of biased PNG and is designed by introducing the impact angle error feedback term. Considering the limit of seeker's field of view, the convergence of the angle error is demonstrated using the Lyapunov-like method. Theoretical analysis shows that the law has finite-time convergence property of the impact angle error w.r.t. range. Furthermore, shaping function is introduced to improve the performance of the proposed guidance scheme.

In this paper, the guidance command is designed as follows

$$a_m = a_{m_{PNG}} + a_{m_{BIS}} \tag{20}$$

where $a_{m_{PNG}}$ has been given in Eq. (10), $a_{m_{BIS}}$ is a biased term and is given by

$$a_{m_{BIS}} = (N-1)\frac{v_m^2}{r}\tan\eta_{\max}\cos\eta f(\eta)\left(\frac{|e_{\phi_f}|}{|(e_{\phi_f})_0|}\right)^{\alpha}\operatorname{sgn}(e_{\phi_f}) \tag{21}$$

where $\alpha \in (0,1)$ is a guidance coefficient, $(e_{\phi_f})_0$ is the impact angle error at initial time t_0. $f(\eta)$ is a continuous shaping function and satisfies

$$f(\eta)\begin{cases} \geq 1, & \text{if} \quad \eta \in (-\eta_{\max}, \eta_{\max}) \\ = 1, & \text{if} \quad \eta = \pm\eta_{\max} \end{cases} \tag{22}$$

Remark 4 Observing from Eqs. (10) and (21), the overall acceleration is theoretically continuous. Although $a_{m_{BIS}}$ contains a signum function, it is weighted by e_{ϕ_f}. And $a_{m_{BIS}}$ will tend to zero as e_{ϕ_f} converges to zero, after that, the guidance command will be the same as PNG.

4.1 Field-of-view constraint satisfaction and Lyapunov stability analysis

To demonstrate the feasibility of the proposed guidance scheme, the concept of invariant set and Lyapunov stability theory are used. The FOV constraint satisfaction and the convergence of impact angle error will be simultaneously considered.

Define the Lyapunov candidate function as

$$V = \frac{1}{2}e_{\phi_f}^2 \tag{23}$$

where V is a function w.r.t. e_{ϕ_f}. Differentiating e_{ϕ_f} in Eq. (6) and combining Eqs. (5), (10), (17), and (20) yield

$$\begin{aligned}\dot{e}_{\phi_f} &= \dot{\hat{\phi}}_f - \dot{\phi}_{f_e} \\ &= \dot{\phi}_{f_{PNG}} \\ &= \dot{\phi} - \frac{N}{N-1}\dot{\eta} \\ &= -\frac{1}{N-1}\frac{a_{m_{BIS}}}{v_m}\end{aligned} \tag{24}$$

Accordingly, the time derivative of v can be calculated by

$$\begin{aligned}\dot{V} &= \dot{e}_{\phi_f} e_{\phi_f} \\ &= -\frac{1}{N-1}\frac{a_{m_{BIS}}}{v_m} e_{\phi_f} \\ &= -\frac{v_m}{r}\tan\eta_{\max}\cos\eta\, f(\eta)|\left(e_{\phi_f}\right)_0|^{-\alpha}|e_{\phi_f}|^{1+\alpha}\end{aligned} \tag{25}$$

Next, it is necessary to analyze the time derivative of leading angle at the boundary of FOV to validate the effectiveness of FOV angle control. Substituting Eq. (20) into Eq. (5) and considering the cases $\eta = \pm\eta_{\max}$ yield

$$\begin{aligned}\dot{\eta}|_{\eta=\pm\eta_{\max}} = \mp(N-1)\frac{v_m}{r}\sin\eta_{\max} \\ \left(1-\left(\frac{|e_{\phi_f}|}{|\left(e_{\phi_f}\right)_0|}\right)^{\alpha}\operatorname{sgn}(e_{\phi_f})\right)\end{aligned} \tag{26}$$

From Eq. (25), $\dot{V}$ is non-positive and equals to zero only at $e_{\phi_f} = 0$. In addition, the interval $\Sigma = [\eta_{\min}, \eta_{\max}]$ is an invariant set of η if $\dot{V}(t) \le 0$ and $\frac{d|\eta|}{dt}|_{\eta=\pm\eta_{\max}} \le 0$ hold for $t \ge t_0$ [15]. As illustrated in Remark 1, η_0 is within the interval Σ, then the conditions $\dot{V}(t) \le 0$ and $\eta(t) \in \Sigma$ for $t \in [t_0, t_f]$ are guaranteed by simultaneously considering the signs of $\dot{V}$ and $\dot{\eta}|_{\eta=\pm\eta_{\max}}$. Accordingly, the proposed guidance scheme could ensure the convergence of the impact angle error while not violating the seeker's FOV limit.

4.2 Guaranteed convergence of impact angle error with respect to range

With further analysis, combining Eqs. (2) and (22), Eq. (25) can be simplified as

$$\begin{aligned}\dot{V} &= (2V)^{\frac{1+\alpha}{2}}\tan\eta_{\max}|\left(e_{\phi_f}\right)_0|^{-\alpha} f(\eta)\frac{\dot{r}}{r} \\ &\le 2^{\frac{1+\alpha}{2}} V^{\frac{1+\alpha}{2}}\tan\eta_{\max}|\left(e_{\phi_f}\right)_0|^{-\alpha}\frac{\dot{r}}{r}\end{aligned} \tag{27}$$

Dividing both sides of Eq. (27) by $V^{\frac{1+\alpha}{2}}$ and rearranging it w.r.t. V and r yield

$$V^{-\frac{1+\alpha}{2}}dV \le 2^{\frac{1+\alpha}{2}}\tan\eta_{\max}|\left(e_{\phi_f}\right)_0|^{-\alpha}\frac{1}{r}dr \tag{28}$$

Integrating both sides of Eq. (28) from V_0 to V and r_0 to r, the relation between V and r is formulated by

$$V^{\frac{1-\alpha}{2}} \le V_0^{\frac{1-\alpha}{2}} + (1-\alpha)2^{-\frac{1-\alpha}{2}}\tan\eta_{\max}|\left(e_{\phi_f}\right)_0|^{-\alpha}\ln\left(\frac{r}{r_0}\right) \tag{29}$$

Notice that $\alpha \in (0,1)$ and $r < r_0$, define r_1 be the relative distance at which e_{ϕ_f} tends to zero, i.e., $r_1 = r|_{e_{\phi_f}=0}$, and r_2 be the relative distance at which the right-hand side of Eq. (29) equals to zero. Note that $r_2 \le r_1$ and r_2 is the lower bound of r_1. Since the inequality Eq. (29) holds, finite-time convergence of the impact angle error is guaranteed as follows

$$V \to 0 \quad \text{as} \quad r \to r_1 \quad (0 < r_2 \le r_1) \tag{30}$$

In this paper, r_2 is designed combining Eq. (29) as follows

$$\begin{aligned}r_1 \ge r_2 &= r_0\exp\left[-\frac{1}{(1-\alpha)\tan\eta_{\max}}|\left(e_{\phi_f}\right)_0|^{\alpha}(2V_0)^{\frac{1-\alpha}{2}}\right] \\ &= r_0\exp\left[-\frac{1}{(1-\alpha)\tan\eta_{\max}}|\left(e_{\phi_f}\right)_0|\right] > 0\end{aligned} \tag{31}$$

Remark 5 It can be seen from the above derivations that $r_2 = r_1$ only if $f(\eta) \equiv 1$. Figure 2 gives the finite-time error convergent property with respect to range. Since $r_2 > 0$, the convergence of error before interception is guaranteed. That is, the problem of impact angle control is solved in this study.

In this paper, shaping function $f(\eta)$ is designed as follows

$$f(\eta) = \left(\frac{\cos\eta}{\cos\eta_{\max}}\right)^{\beta} \tag{32}$$

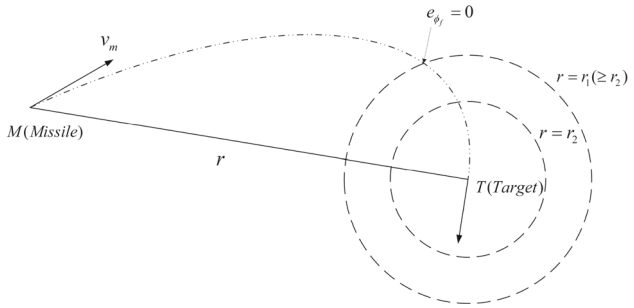

Fig. 2 Finite-time error convergence with respect to range

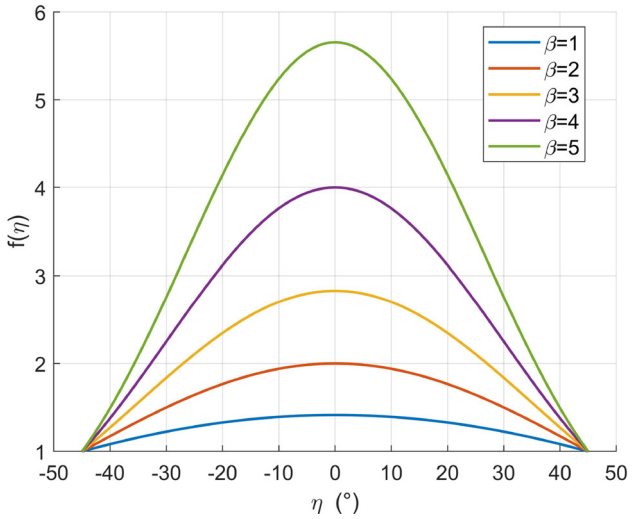

Fig. 3 Shaping function

where

$$\beta = k\left(\frac{\cos\eta_0}{\sin\eta_{\max}}\frac{\pi}{|\left(e_{\phi_f}\right)_0|}\right)^p \tag{33}$$

In Eq. (33), k, p, and β are non-negative constants, the shaping function meets the condition given in Eq. (22).

Remark 6 The dynamic characteristics of shaping function $f(\eta)$ with respect to leading angle η are depicted in Fig. 3, different values of coefficient β ($\beta = 1, 2, 3, 4, 5$) are also investigated to show their effect on the shaping function. It can be seen from Fig. 3 that $f(\eta) \geq 1$ holds for different β; as β increases, the value of $f(\eta)$ also increases, and the generated trajectory is more curved. The influence of shaping function on the proposed guidance scheme will be simulated and analyzed in detail in Sect. 5.

5 Simulations

In this section, simulations are conducted to validate the performance and characteristics of the proposed guidance law. The influence of shaping function is first presented. The scenario of different expected impact angles with shaping function is also conducted; comparative study with existing relative works is performed at last.

To avoid possible command chattering and generate a smoother guidance command, it is worth noting that signum function in Eq. (21) is improved and modified by a hyperbolic tangent function selected as follows

$$\tanh(x) = \frac{2}{1+\exp(-2ax)} - 1 \tag{34}$$

The engagement conditions including initial settings and physical constraints are summarized in Table 1. Guidance parameters are selected as follows: $N = 3, k = 10, p = 1, \alpha = 0.1, a = 10$. The fourth-order Runge–Kutta method is used in this study with step length being 0.001 s. $r < 1$m is designed as the termination condition of the simulation.

Table 1 Engagement conditions for numerical simulation

Parameters	Values
Missile initial position	$(-10,000, 0)$m
Target position	(0,0)m
Seeker's FOV (Σ)	[–45°,45°]
Launch angle ($\phi_0 = \eta_0$)	30°

5.1 Shaping function effect

First of all, the guidance performance with and without shaping function is analyzed. The expected impact angle is $\phi_{f_e} = -90°$. When shaping function is not used, $f(\eta)$ equals to 1. The simulation results are presented in Fig. 4. Figure 4a gives the guidance trajectories, the black solid line represents the trajectory with shaping function, while the red dotted line represents the trajectory without shaping function. Both cases can hit the stationary target, and the trajectory with shaping function is more curved. Figure 4b gives the FPA histories, the terminal FPA under two cases are all equal to nearly $-90°$, with error being very small, which shows that the angle constraint is well addressed. Leading angle histories are plotted in Fig. 4c; since the FOV upper boundary is 45°, it can be seen that the dynamics of η change more dramatically under the effect of shaping function, and both cases meet the FOV requirement. What is more, the leading angles tend to zero finally, which validates the property conducted in Remark 1. Figure 4d gives the impact angle error histories, the errors of black and red converge to zero at 38.328 s and 40.041 s, respectively, and the relative distances at these two time instants are 1236.7681 m and 373.4906 m. The overall flight times are 42.456 s and 41.283 s. This indicates that the introduction of shaping function could lengthen the distance

Fig. 4 Shaping function effect

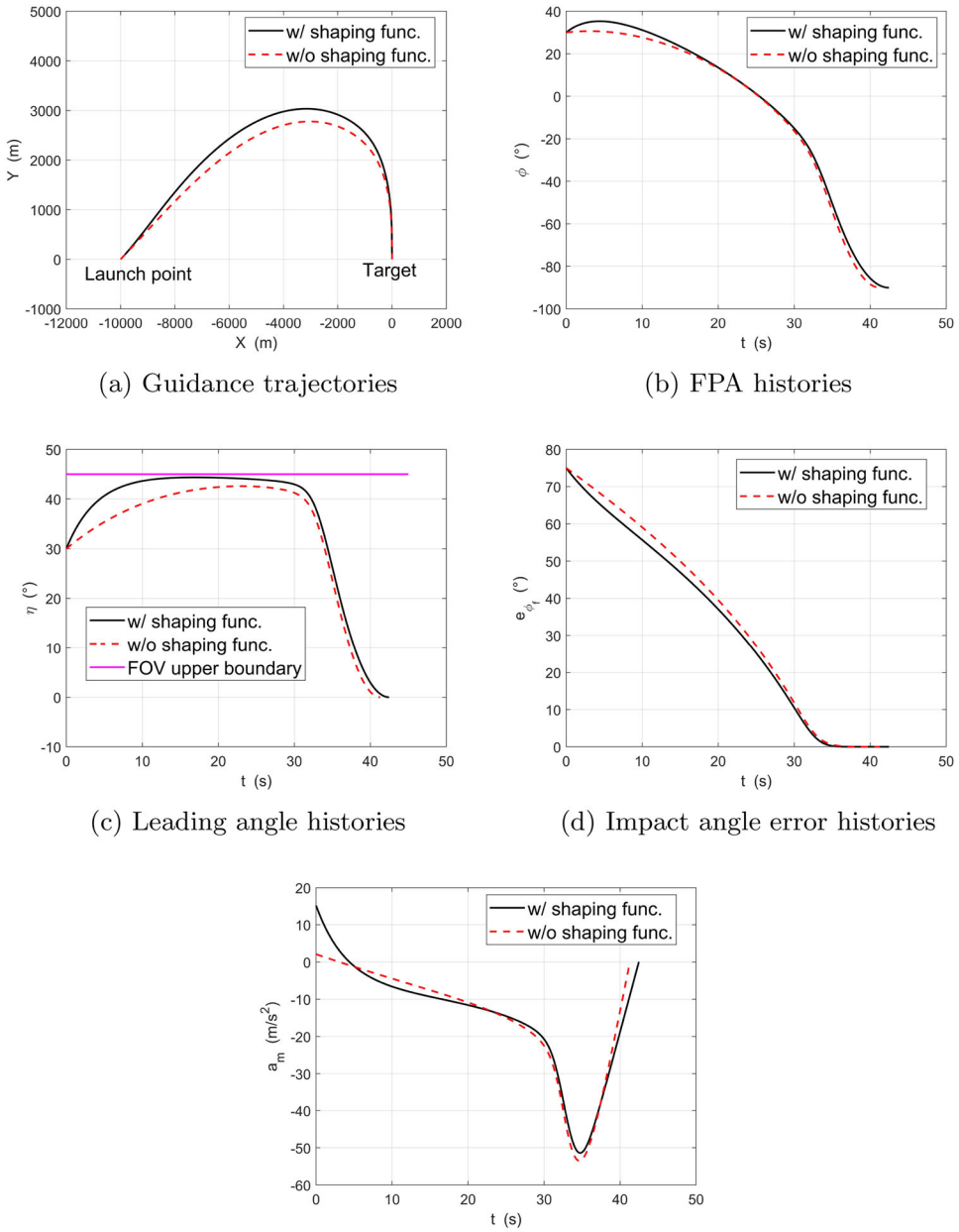

(a) Guidance trajectories

(b) FPA histories

(c) Leading angle histories

(d) Impact angle error histories

(e) Guidance command histories

at which error becomes zero. Figure 4e presents the guidance command histories, the commands under two cases are continuous and finally tend to zero. The indexes of the shaping function effect including miss distance are summarized in Table 2.

5.2 Different expected impact angles with shaping function

Considering another scenario that the missile attacks the target at different expected impact angles with shaping function. The ϕ_{ef} is chosen as -60°, -90°, and -120°, respectively. The results are summarized in Fig. 5. Figure 5a shows that the second half of the guidance trajectories varies differently to meet the constraint requirement. Figure 5b gives the FPA histories, the impact angle can be controlled at least within the interval of $[-120°, -60°]$ with high accuracy. Figure 5c presents the leading angle trends, the FOV angle control is further validated in this scenario. Impact angle error histories are shown in Fig. 5d, it can be seen that the error convergence rate gets slower as the magnitude of ϕ_{ef} increases. Guidance command variations are plotted in Fig. 5e.

Table 2 Shaping function effect

Indexes	With shaping function	Without shaping function
Overall flight time t_f (s)	42.456	41.283
The time instant that $e_{\phi_f} = 0$ (s)	38.328	40.041
r_1 (m)	1236.7681	373.4906
Miss distance (m)	0.8278	0.8938

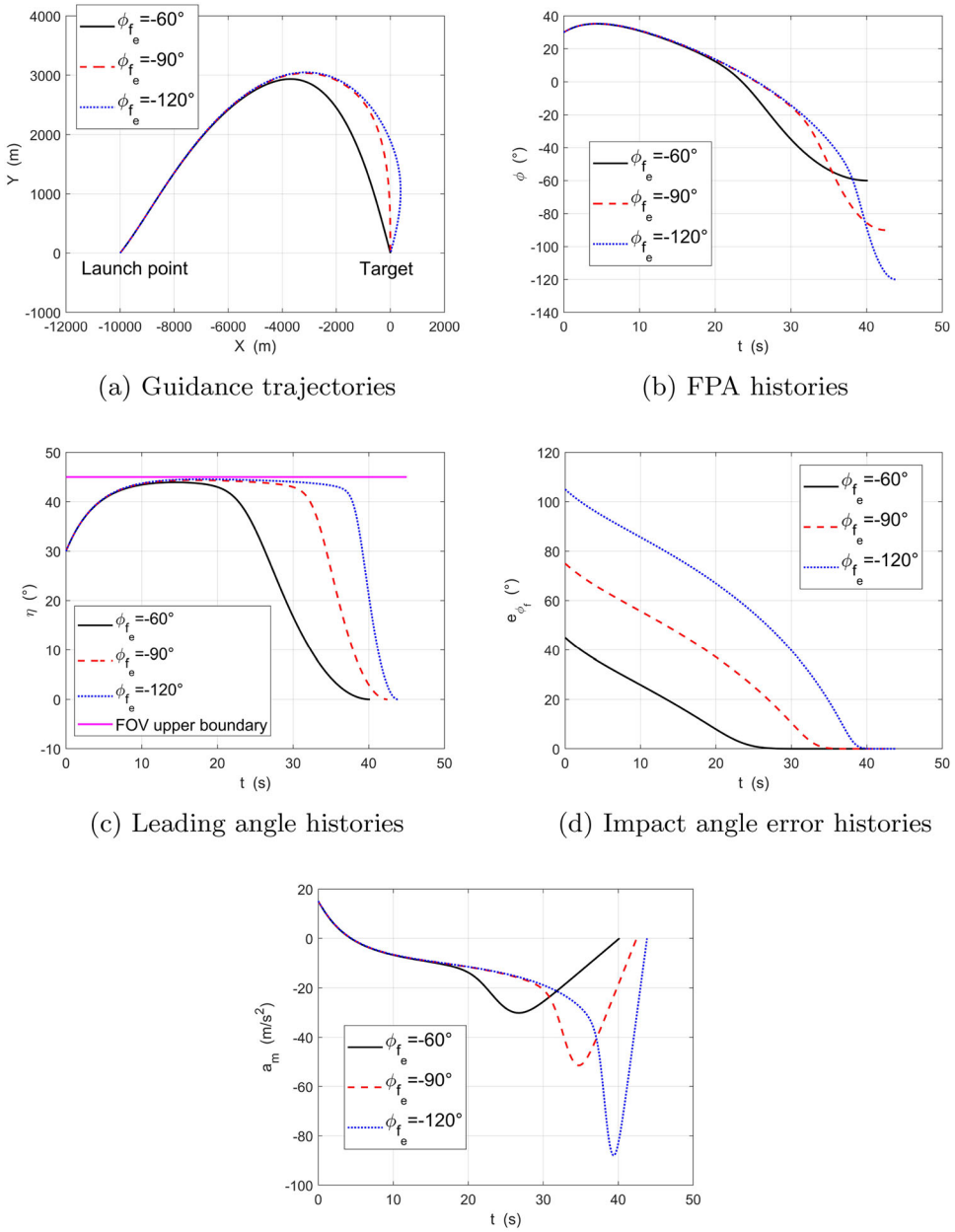

Fig. 5 Different expected impact angles

(a) Guidance trajectories

(b) FPA histories

(c) Leading angle histories

(d) Impact angle error histories

(e) Guidance command histories

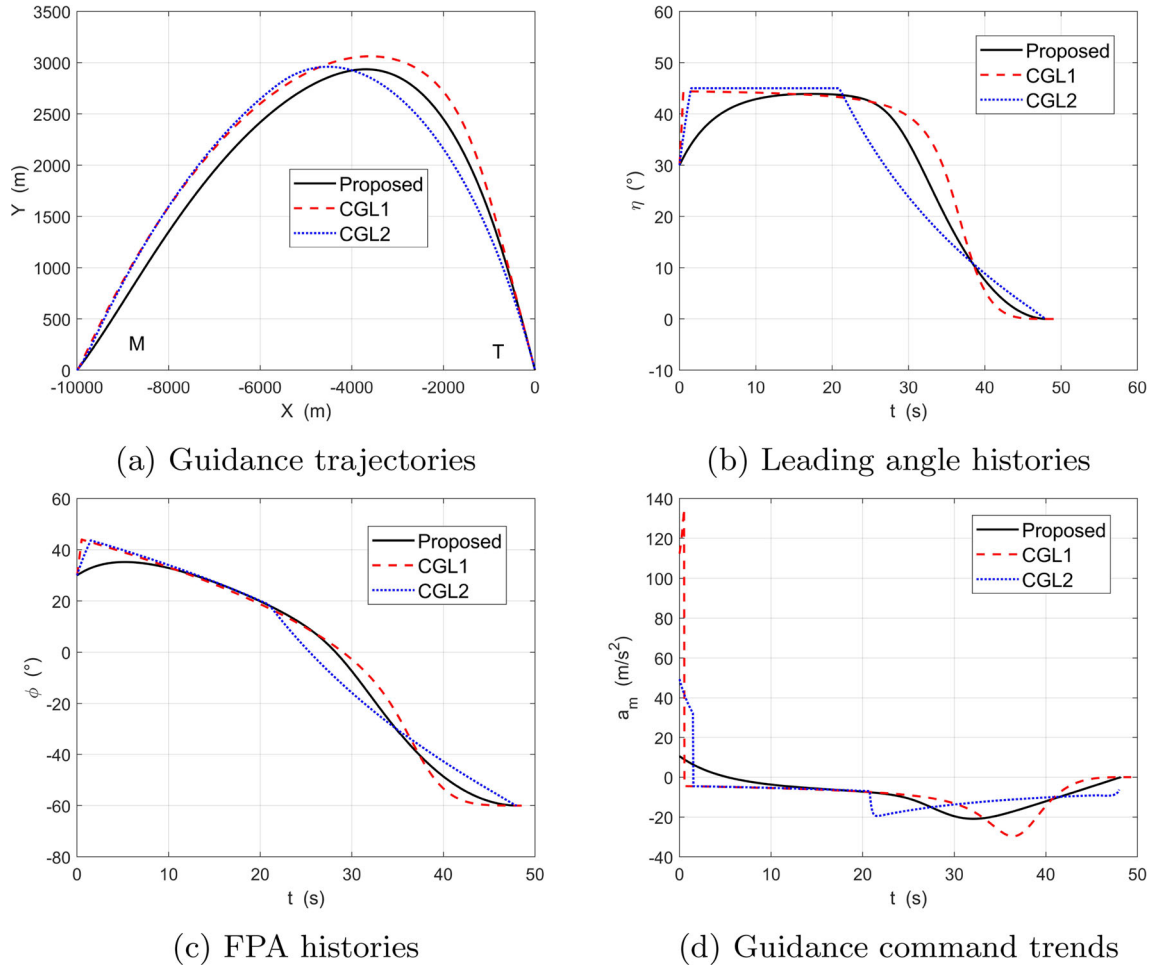

(a) Guidance trajectories (b) Leading angle histories

(c) FPA histories (d) Guidance command trends

Fig. 6 Comparative results with $\phi_{f_e} = -60°$

5.3 Comparative study

Comparative study is conducted in this subsection to test the advantages of the proposed guidance scheme. For fair comparison, two new relative works with both angle and FOV constraints are investigated [27] and [28]. Ref. [27] uses sliding mode control to address the two constraints with unknown disturbance (denoted as CGL1). While Ref. [28] is the latest published and performs a two-stage guidance framework. FOV constraint is solved based on the principle of switching logic. Denote [28]'s law as 'CGL2', comparative results are presented in Figs. 6 and 7. Notice that the missile speed is set as 250 m/s in each law, the guidance parameters are the same as given in Refs. [27] and [28]. To show the differences, two engagement scenarios with $\phi_{f_e} = -60°$ and $\phi_{f_e} = -110°$ are conducted, respectively.

Figure 6a gives the guidance trajectories of three laws under the condition $\phi_{f_e} = -60°$, the trajectories show different curvatures and the target can be successfully intercepted. Figure 6b presents the leading angle histories, the proposed law as marked in black line can make the angle vary within the boundary 45°; the CGL1 as marked in red line makes the leading angle reach to nearly 45° at the very beginning and then gradually converge to zero; while under the CGL2, owing to the two stage property, when the leading angle reaches the boundary, it will stay on this value until the switching logic is triggered and then tend to zero. To conclude, the proposed law shows better performance in leading angle variation, the angle changes more smoother compared with the other two laws. Figure 6c gives the FPA histories, the impact angles under three laws can be successfully controlled to $-60°$ in this case. Moreover, Fig. 6d presents the guidance command trends, since the guidance command is a vital variable in the guidance and control loop design of missile, the command should be as smooth as possible and the magnitude should not be large. The proposed law shows good acceleration variation while the CGL1 has command chattering at about 0.5 s and the magnitude reaches to more than $12g$, which is not reasonable for practical engineering. The CGL2 also generates discontinuous command at about 1.9 s and 22.3 s as

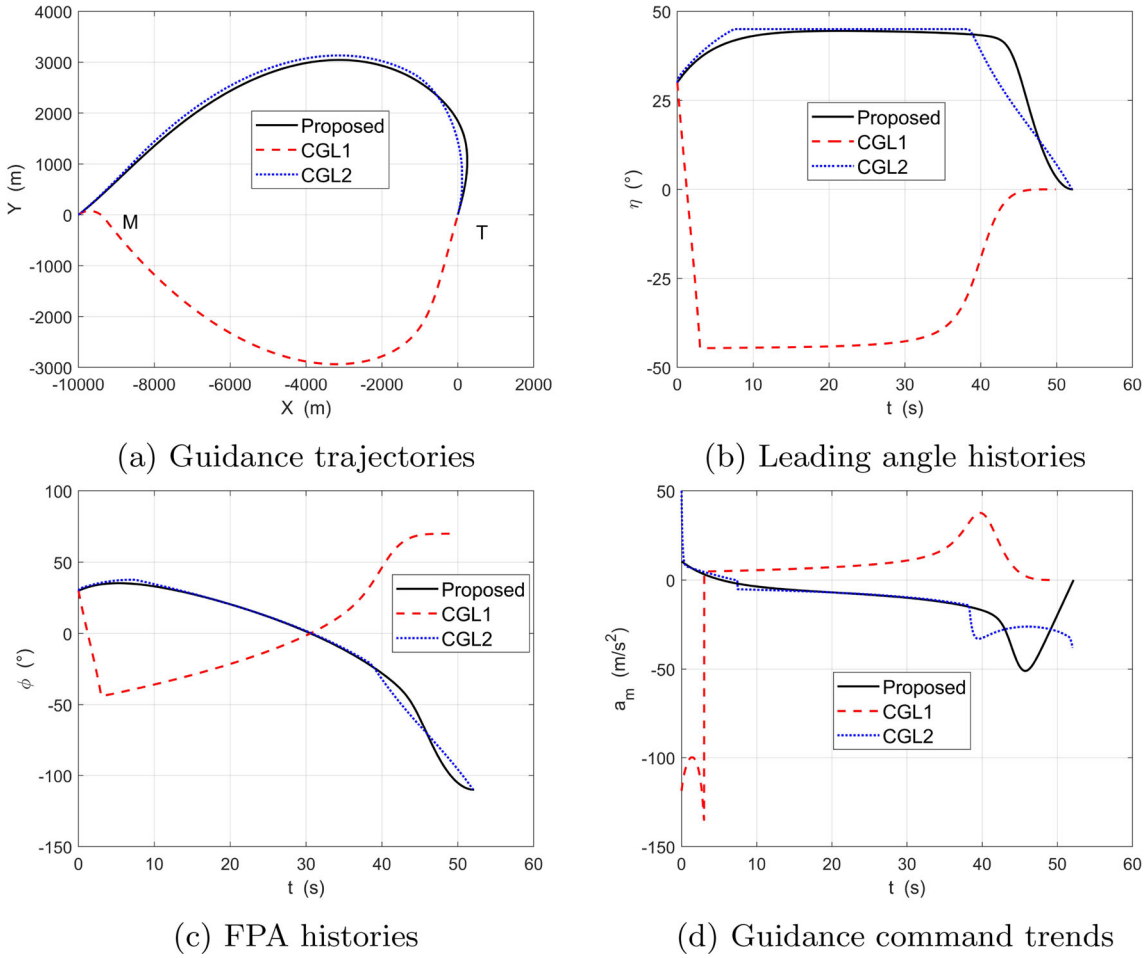

(a) Guidance trajectories (b) Leading angle histories

(c) FPA histories (d) Guidance command trends

Fig. 7 Comparative results with $\phi_{f_e} = -110°$

Table 3 Comparison of three laws

Indexes	Impact angle error (°)	Control effort (m^2/s^3)	Miss distance (m)
Scenario $\phi_{f_e} = -60°$, Proposed	0.0001	2892.8	0.7326
Ref. [27]'s law	0.0002	7191.1	0.8261
Ref. [28]'s law	0.0012	3813.5	0.7156
Scenario $\phi_{f_e} = -120°$, Proposed	0.0001	7917.2	0.6335
Ref. [27]'s law	180.0022	22007.1	0.8126
Ref. [28]'s law	0.0017	6930.8	0.7297

shown from the figure, this can be attributed to the switching logic used in it.

As for the other scenario $\phi_{f_e} = -110°$, Fig. 7a indicates that three laws can guide the missile hit the target. From Fig. 7b, c, it can be seen that Ref. [27]'s law fails to meet terminal FPA requirement as the ϕ_{f_e} is set as $-110°$, the other two laws have good performance. The FOV angles are well controlled under three laws. Figure 7d presents the acceleration variations, the analysis can be similar to Fig. 6d, the proposed law generates much smoother command than the other two laws. Considering the control effort (CE) of missile which can be calculated by $\text{CE} = \frac{1}{2}\int_{t_0}^{t_f} |a_m|^2 dt$, the comparison of three guidance laws under the two scenarios from different perspectives is concluded in Table 3.

When $\phi_{f_e} = -60°$, the impact angle errors of the above three laws are almost zero, which shows good angle control in this case. The control effort has the relation of proposed < CGL2 < CGL1, and the miss distances are all less than 1 m. As for $\phi_{f_e} = -110°$, the proposed and Ref. [28]'s laws can fulfill the angle constraint with high accuracy, but Ref. [27]'s

law fails to meet the requirement. The error is 180.0022 °, this can be the limitation of Ref. [27]'s law that it may not be applicable to large angle interceptions. The control effort relation in this case is CGL2 < proposed < CGL1, the proposed law generates bigger control effort than CGL2, but it is much smaller than CGL1's law. In summary, the proposed law has good performance in impact angle control and control effort consumption. Most importantly, the command derived in this study is much smoother and reasonable.

6 Conclusion

A PNG-based guidance law with FOV and angle constraints is proposed in this study. The basic principles of PNG are first introduced and the terminal flight path angle is derived based on it to formulate the angle error. By designing an error feedback controller with the form of biased term, the two constraints are well addressed. The proposed law is essentially a biased PNG which can make the missile hit the target as long as the biased term becomes zero before interception. The finite-time error convergence is demonstrated and guaranteed via a Lyapunov-like approach. Finally, numerical simulations with a comparative study validate the effectiveness and strengths of the proposed law. Future works can extend the two-dimensional engagement scenario to a three-dimensional one under multiple constraints; besides, the autopilot lag and some other disturbances should also be considered.

Funding This work was supported by the Shanghai Academy of Spaceflight Technology and Shanghai Jiao Tong University (SAST-SJTU) Advanced Space Technology Joint Research Fund (No. USCAST 2020-8), and the National Natural Science Foundation of China (No. U20B2054).

Data Availability The data including code will be made available from the corresponding author on reasonable request.

Declarations

Conflict of interest The authors have not disclosed any competing interests.

References

1. Lee J-I, Jeon I-S, Tahk M-J (2007) Guidance law to control impact time and angle. IEEE Trans Aerosp Electron Syst 43(1):301–310. https://doi.org/10.1109/TAES.2007.357135
2. Wang X, Lu H, Huang X, Zuo Z (2021) Three-dimensional terminal angle constraint finite-time dual-layer guidance law with autopilot dynamics. Aerosp Sci Technol 116:106818. https://doi.org/10.1016/j.ast.2021.106818
3. Ryoo C-K, Cho H, Tahk M-J (2005) Optimal guidance laws with terminal impact angle constraint. J Guid Control Dyn 28(4):724–732. https://doi.org/10.2514/1.8392
4. Ryoo C-K, Cho H, Tahk M-J (2006) Time-to-go weighted optimal guidance with impact angle constraints. IEEE Trans Control Syst Technol 14(3):483–492. https://doi.org/10.1109/TCST.2006.872525
5. Yang C-D, Chen H-Y (1998) Nonlinear h robust guidance law for homing missiles. J Guid Control Dyn 21(6):882–890. https://doi.org/10.2514/2.4321
6. Bardhan R, Ghose D (2015) Nonlinear differential games-based impact-angle-constrained guidance law. J Guid Control Dyn 38(3):384–402. https://doi.org/10.2514/1.G000940
7. Kim H-G, Cho D, Kim HJ (2018) Sliding mode guidance law for impact time control without explicit time-to-go estimation. IEEE Trans Aerosp Electron Syst 55(1):236–250. https://doi.org/10.1109/TAES.2018.2850208
8. Kumar SR, Rao S, Ghose D (2012) Sliding-mode guidance and control for all-aspect interceptors with terminal angle constraints. J Guid Control Dyn 35(4):1230–1246. https://doi.org/10.2514/1.55242
9. Cho D, Kim HJ, Tahk M-J (2015) Impact angle constrained sliding mode guidance against maneuvering target with unknown acceleration. IEEE Trans Aerosp Electron Syst 51(2):1310–1323. https://doi.org/10.1109/TAES.2015.140358
10. Mishley A, Shaferman V (2022) Linear quadratic guidance laws with intercept angle constraints and varying speed adversaries. J Guid Control Dyn 45(11):2091–2106. https://doi.org/10.2514/1.G006776
11. He S, Lin D, Wang J (2018) Integral global sliding mode guidance for impact angle control. IEEE Trans Aerosp Electron Syst 55(4):1843–1849. https://doi.org/10.1109/TAES.2018.2876588
12. Chen Y, Wu S, Wang X (2022) Impact time and angle control optimal guidance with field-of-view constraint. J Guid Control Dyn 45(12):2369–2378. https://doi.org/10.2514/1.G007030
13. Dong W, Wang C, Wang J, Son H, Xin M (2022) Unified method for field-of-view-limited homing guidance. Journal of Guidance, Control, and Dynamics, 1–20. https://doi.org/10.2514/1.G006710
14. Lee S, Kim Y (2020) Capturability of impact-angle control composite guidance law considering field-of-view limit. IEEE Trans Aerosp Electron Syst 56(2):1077–1093. https://doi.org/10.1109/TAES.2019.2925485
15. Wang X, Zhang Y, Wu H (2016) Sliding mode control based impact angle control guidance considering the field-of-view constraint. ISA Trans 61:49–59. https://doi.org/10.1016/j.isatra.2015.12.018
16. Wang J, Ding X, Chen Y, Wang C, Xin M (2022) Field-of-view constrained three-dimensional impact angle control guidance for speed-varying missiles. IEEE Trans Aerosp Electron Syst 58(5):3992–4003. https://doi.org/10.1109/TAES.2022.3157807
17. Liu B, Hou M, Yu Y, Wu Z (2020) Three-dimensional impact angle control guidance with field-of-view constraint. Aerosp Sci Technol 105:106014. https://doi.org/10.1016/j.ast.2020.106014
18. Chen Y, Wu S, Wang X, Zhang D, Jia J, Li Q (2023) Time and fov constraint guidance applicable to maneuvering target via sliding mode control. Aerospace Science and Technology, 108104. https://doi.org/10.1016/j.ast.2023.108104
19. Cho N, Kim J, Lee S, Kim Y (2022) Generalized analysis of biased proportional navigation guidance with fractional power error feedback. Journal of Guidance, Control, and Dynamics, 1–16. https://doi.org/10.2514/1.G006850
20. Chen Y, Wang J, Wang C, Shan J, Xin M (2020) Three-dimensional cooperative homing guidance law with field-of-view constraint. J Guid Control Dyn 43(2):389–397. https://doi.org/10.2514/1.G004681
21. Han T, Hu Q, Xin M (2020) Analytical solution of field-of-view limited guidance with constrained impact and capturability analysis. Aerosp Sci Technol 97:105586. https://doi.org/10.1016/j.ast.2019.105586

22. Hu Q, Han T, Xin M (2020) Analytical solution for nonlinear three-dimensional guidance with impact angle and field-of-view constraints. IEEE Trans Industr Electron 68(4):3423–3433. https://doi.org/10.1109/TIE.2020.2982114
23. Han T, Hu Q, Xin M (2022) Three-dimensional approach angle guidance under varying velocity and field-of-view limit without using line-of-sight rate. IEEE Transactions on Systems, Man, and Cybernetics: Systems 52(11):7148–7159. https://doi.org/10.1109/TSMC.2022.3150299
24. Han T, Hu Q, Shin H-S, Tsourdos A, Xin M (2021) Sensor-based robust incremental three-dimensional guidance law with terminal angle constraint. J Guid Control Dyn 44(11):2016–2030. https://doi.org/10.2514/1.G006038
25. Liu B, Hou M, Li Y (2019) Field-of-view and impact angle constrained guidance law for missiles with time-varying velocities. IEEE Access 7:61717–61727. https://doi.org/10.1109/ACCESS.2019.2916798
26. Zhou S, Zhang S, Wang D (2020) Impact angle control guidance law with seeker's field-of-view constraint based on logarithm barrier lyapunov function. IEEE Access 8:68268–68279. https://doi.org/10.1109/ACCESS.2020.2986355
27. Kim H-G, Kim HJ (2020) Field-of-view constrained guidance law for a maneuvering target with impact angle control. IEEE Trans Aerosp Electron Syst 56(6):4974–4983. https://doi.org/10.1109/TAES.2020.2996306
28. Yang X, Zhang Y, Song S (2023) Two-stage cooperative guidance strategy with impact-angle and field-of-view constraints. J Guid Control Dyn 46(3):590–599. https://doi.org/10.2514/1.G007040